Naval Research Laboratory

Washington, DC 20375-5320

NRL/MR/6110--11-9372

Transient Electromagnetic Wave Propagation in a Plasma Waveguide

HAROLD D. LADOUCEUR

Chemical Dynamics and Diagnostics Branch
Chemistry Division

ANDREW P. BARONAVSKI

Envisioneering, Inc.
King George, Virginia

October 24, 2011

REPORT DOCUMENTATION PAGE

Form Approved
OMB No. 0704-0188

1. REPORT DATE *(DD-MM-YYYY)*	**2. REPORT TYPE**	**3. DATES COVERED** *(From - To)*
24-10-2011	Memorandum	October 2010 - September 2011

4. TITLE AND SUBTITLE

Transient Electromagnetic Wave Propagation in a Plasma Waveguide

5a. CONTRACT NUMBER

5b. GRANT NUMBER

5c. PROGRAM ELEMENT NUMBER

6. AUTHOR(S)

Harold D. Ladouceur and Andrew P. Baronavski*

5d. PROJECT NUMBER

5e. TASK NUMBER
MA013-01-44

5f. WORK UNIT NUMBER
4250

7. PERFORMING ORGANIZATION NAME(S) AND ADDRESS(ES)

Naval Research Laboratory, Code 6111
4555 Overlook Avenue, SW
Washington, DC 20375-5320

8. PERFORMING ORGANIZATION REPORT NUMBER

NRL/MR/6110--11-9372

9. SPONSORING / MONITORING AGENCY NAME(S) AND ADDRESS(ES)

Office of Naval Research
One Liberty Center
875 North Randolph Street
Arlington, VA 22203-1995

10. SPONSOR / MONITOR'S ACRONYM(S)

ONR

11. SPONSOR / MONITOR'S REPORT NUMBER(S)

12. DISTRIBUTION / AVAILABILITY STATEMENT

Approved for public release; distribution is unlimited.

13. SUPPLEMENTARY NOTES

*Envisioneering, Inc., 4485 Danube Drive, Suite 46, King George, VA 22485

14. ABSTRACT

An analytic model to describe the transient propagation of an electromagnetic wave inside a hollow constant conductivity plasma annular tube is formulated. The model neglects external radiative emission since the plasma tube wall is assumed to be several skin depths in thickness. Approximate analytic time-dependent solutions for mode propagation are obtained by a combination of integral transform techniques and the method of eigenfunction expansion with homogeneous boundary conditions. The model provides insight into wave attenuation, the dispersion relations, waveguide excitation and mode coupling due to finite wall plasma conductivity. The model is developed by first considering the transient propagation characteristics of ideal cylindrical waveguides with perfectly conducting walls. This preliminary analysis provides a consistent notation for the closed plasma waveguide and suggests possible launching modes with minimal loss. The initial condition imposed on the annular plasma waveguide is fixed by exciting a specified mode in the ideal cylindrical waveguide which is then transferred into the plasma tube.

15. SUBJECT TERMS

Plasma waveguide
Transient wave propagation
Green's function
Modal expansion techniques
Transient propagator
Laser-induced plasma filament
Femtosecond laser

16. SECURITY CLASSIFICATION OF:			**17. LIMITATION OF ABSTRACT**	**18. NUMBER OF PAGES**	**19a. NAME OF RESPONSIBLE PERSON**
a. REPORT	**b. ABSTRACT**	**c. THIS PAGE**			Harold D. Ladouceur
Unclassified	Unclassified	Unclassified	UU	29	**19b. TELEPHONE NUMBER** *(include area code)* (202) 767-3558

CONTENTS

EXECUTIVE SUMMARY

A number of papers have appeared in the open literature describing either experimental or theoretical work using laser induced filaments to guide energy in the form of microwave radiation. The idea is to minimize the natural divergence of a radiation source by confining the energy flow in a specified direction with the aide of conducting plasma filaments which would maintain a high energy density over a large distance. The filaments act either as an open waveguide (Goubau line) or they can be arranged to form a hollow plasma tube. The theoretical work published to date in the open literature assumes steady-state plasma with constant conductivity. In reality, the plasma decays within tens of nanoseconds due to recombination and electron attachment. Thus, the correct theoretical treatment of the problem should take into account the transient effects involved in both the launching of the electromagnetic wave and the simultaneous loss of plasma conductivity. The transient launching problem is considered here.

An analytic model to describe the *transient* propagation of an electromagnetic wave inside a hollow constant conductivity plasma annular tube is formulated. The model neglects external radiative emission since the plasma tube wall is assumed to be several skin depths in thickness. Approximate analytic time-dependent solutions for mode propagation are obtained by a combination of integral transform techniques and the method of eigenfunction expansion with homogeneous boundary conditions. The model provides insight into wave attenuation, the dispersion relations, waveguide excitation and mode coupling due to finite wall plasma conductivity. The model is developed by first considering the transient propagation characteristics of ideal cylindrical waveguides with perfectly conducting walls. This preliminary analysis provides a consistent notation for the closed plasma waveguide and suggests possible launching modes with minimal loss. The initial condition imposed on the annular plasma waveguide is fixed by exciting a specified mode in the ideal cylindrical waveguide which is then transferred into the plasma tube.

The propagation problem with Joule heating within the plasma tube wall is analyzed numerically using a finite-element technique and some preliminary results are given.

Transient Electromagnetic Wave Propagation in a Plasma Waveguide

I. INTRODUCTION

A number of experimental and theoretical papers have appeared in the open literature describing the use of laser-induced filaments to guide energy in the form of microwave radiation[1-5]. The natural divergence of a radiation source can be reduced if the energy flow is confined within a limited spatial region by walls (closed waveguide) or a guiding structure such as a parallel transmission line. The simplest open-guide structure is a single dielectric coated wire of *finite* conductivity known as a Goubau line[6]. The electromagnetic energy is transported along this open line as an attached surface wave. The propagation of the surface wave depends upon the ability of the electromagnetic field to penetrate the conductor's interior. A *perfect* single conductor will not support such a guided wave. The propagation characteristics of the guided wave are determined by the wire conductivity, the wire radius, and the radiation frequency. The guiding performance is enhanced by coating the wire with a dielectric. The calculation of the propagation characteristics is based upon tangential continuity of the electric and magnetic field components across the dielectric-wire surface boundary and utilizes a *steady-state* sinusoidal approximation. The standard analysis neglects how the wave was launched.

The laser-induced plasma filaments behave as ohmic resistors over distances on the order of tens of centimeters[7]. By treating a single filament as a time-dependent resistance, we have determined the electron density, the kinetic parameters for electron attachment and recombination, and an effective conductivity of 350 S/m. In order to arrive at this conductivity, we assumed that the filament was a cylinder with a diameter on the order of 100 μm and that the plasma electrons had a collision frequency of 10^{12} s^{-1}. Later experiments conducted at NRL obtained the conductivity by a technique which does not require knowledge of the electron collision frequency. The initial filament conductivity is 50 S/m and decays to 4-5 S/m over a few hundred nanoseconds.

The laser is a conventional chirped pulse amplified Ti:Sapphire laser. A KML oscillator is stretched and amplified to about 1.5 mJ in a Coherent Spitfire regenerative amplifier at 1 kHz. These pulses are then amplified by a Coherent custom built frequency doubled Nd:YAG laser in a four pass amplifier to about 1.2 Joules in ~260 picosec at 10 Hz repetition rate. The stretched pulses are expanded to 40 mm diameter and compressed with dual gold coated gratings resulting in 40 femtosec, 850 mJ pulses. A simple two mirror telescope is used to control the spot size down stream from the laser and the position of filament formation is controlled by adjusting the grating separation. Typically, spot sizes on the order of 1 – 1.5 cm diameter are used in the experiments and contain 70-80 filaments. Although the filament distribution can change from day to day, normally once the system has stabilized (after 40 minutes) the distribution remains the same for the rest of the day.

In any experiment attempting to use the laser-induced filaments as a guiding structure, the transient behavior of the plasma and the electromagnetic interaction within the particular experimental configuration must be understood in order to correctly interpret the results. The NRL femtosecond laser is capable of consistently producing 75-80 filaments within a one centimeter diameter disk at ten hertz frequency over several meters. The filaments are "produced" on a time scale of a few nanoseconds over the experimental geometry. The electromagnetic field measurements are on the same time scale. Thus, all of our observations involve transient processes and the standard steady-state approximation of sinusoidal waves is inapplicable in theoretical or experimental work with short-lived laser-induced filaments. This report documents our current progress in developing such transient models.

An alternative experimental approach which can avoid the transient plasma lifetime to some extent is to create the plasma in air by focusing high-energy laser beams. There are several published

Manuscript approved September 25, 2011.

papers that use this technique[8-12]. Plasmas created in this manner do not contain the laser-generated filaments produced by self-focusing and require enormous energy. The electron density is lower and creation of the plasma may require seeding the atmosphere with a hydrocarbon. Microwave radiation has been guided over a distance of 60 m at 35.3 GHz frequency by a closed waveguide created in this fashion[8-9]. However, we believe that the energy cost (50 J) and the complexity of the KrF excimer laser used in the experiment as well as the required optics would be offset by simply using a larger microwave source.

In order to develop a transient model of the electromagnetic interaction with the plasma, an experimental configuration must be selected for the analysis. Since we are interested in guiding the energy, a simple circular metal waveguide coupled to a hollow plasma tube whose walls are several skin depths in thickness was selected as a preliminary base line model. The metal waveguide provides an initial condition for the propagation of the wave into the plasma tube. If the experimental geometry were changed to a circular horn for example, the same mathematical technique described here should still be applicable. The basis sets used in the model would be modified to the appropriate geometry and coordinate system.

Section II develops the notation, dispersion relations, and description of the modes and cut off frequencies for the ideal circular waveguide. This notation is utilized in Section III for the development of the time-dependent theory. If the reader is familiar with these concepts he should be able to skip Section II and proceed to the transient analysis in Section III.

II. STEADY-STATE WAVEGUIDE THEORY

The propagation of electromagnetic radiation in a lossy waveguide is governed by Maxwell's equations. The analytic solution of the Maxwell equations provides the axial propagation constant for the radiation field, the eigenvalues and eigenfunctions associated with a particular mode for the specified geometry (waveguide cross section), and the waveguide dispersion relation as a function of geometry and frequency. The attenuation due to finite-wall conductivity is often treated as a perturbation of the perfect wall conductor solutions. Transient effects are customarily neglected, since steady-state sinusoidal solutions are most often of practical engineering interest. Losses due to the dielectric (air) within the guide are usually negligible.

The standard engineering procedure in solving the waveguide problem for a sinusoidal input source is to transform the Maxwell equations to a coordinate system appropriate to the waveguide geometry and then assume that the waveguide walls are perfect conductors[14]. The assumption of perfect wall conductivity simplifies the imposition of the boundary conditions. The tangential component of the electric field and the normal component of the magnetic field intensity must vanish at the waveguide wall. These boundary conditions impose the mode structure and "restrict" the propagation of the radiation field to the interior of the guide. In reality the electromagnetic wave penetrates the wall, but is exponentially attenuated over a radial distance of a few skin depths. The skin depth $\delta(f,\sigma)$ is given by

$$\delta(f,\sigma) = \sqrt{\frac{1}{\mu_0 \pi f \sigma}} \tag{1.1}$$

f denotes the radiation frequency and σ the wall conductivity. Equation (1.1) shows that at higher frequencies and/or wall conductivities the skin depth decreases and there is less wall penetration of the radiation field. At gigahertz frequencies the skin depth in a good conductor such as copper with conductivity $\approx 10^7$ S/m is on the order of microns. Note that the waveguide wall thickness should be at least 2-3 times the skin depth in order to confine the radiation field and provide a guiding structure. If the wall conductivity is too low, the radiation field can "leak" out of the waveguide into the surrounding free space.

In the analysis of guided waves along uniform systems, it is customary to classify the wave solutions into the following three types:

1. *Transverse electromagnetic waves (TEM)* These waves have their electric and magnetic field components entirely in the transverse plane. There is neither an electric nor magnetic field component in the propagation direction. TEM waves propagate on multi-conductor guides such as transmission lines and are sometimes called *principal waves*. The TEM mode does not exist inside a single, hollow, cylindrical conductor of infinite conductivity and will not be considered any further.
2. *Transverse magnetic waves (TM)* In a TM wave there is an electric field component (E_z) along the direction of wave propagation. The magnetic field component lies entirely within the transverse plane. TM waves may also have transverse electric components, e.g., E_x, E_y or E_ϕ. These waves are sometimes called E waves in the literature.
3. *Transverse electric waves (TE)* In a TE wave there is an axial component of the magnetic field (H_z) along the propagation direction. The transverse plane may have both electric and magnetic field components. These waves are also referred to as H waves.

We will first review some elementary results for a hollow, cylindrical conductor of infinite conductivity. These results provide a zero-order solution for the transient model, establish the notation and give insight into the mathematical issues that arise in developing the transient model of the plasma waveguide. Moreover, a cylindrical metal waveguide provides a possible launching device for a specified mode. The judicious selection of a low-loss launching mode may enhance the performance of the plasma waveguide.

Electric and magnetic fields are **vecto**r quantities, which are related in space and time via Maxwell's equations

$$\begin{aligned} \nabla \cdot \vec{D} &= \rho \qquad & \nabla \times \vec{E} &= -\frac{\partial \vec{B}}{\partial t} \qquad & \vec{D} &= \varepsilon_0 \vec{E} \\ \nabla \cdot \vec{B} &= 0 \qquad & \nabla \times \vec{H} &= \vec{J} + \frac{\partial \vec{D}}{\partial t} \qquad & \vec{B} &= \mu_0 \vec{H} \end{aligned} \tag{2.1}$$

The standard mathematical technique in solving the steady-state sinusoidal waveguide problem is to assume *a priori* that the vector solution can be written in the following form

$$\begin{aligned} \vec{E}(x,y,z,t) &= \vec{E}(x,y)\exp\left[\, j\omega t - kz \right] \\ \vec{B}(x,y,z,t) &= \vec{B}(x,y)\exp\left[\, j\omega t - kz \right] \end{aligned} \tag{2.2}$$

Traveling or standing waves in the axial direction (z) can be described by taking appropriate linear combinations of the exponential functions. The parameter k is the propagation constant or wave number and may be real or complex. Substitution of equation (2.2) into (2.1) yields a two-dimensional vector Helmholtz equation. The dispersion relation $k(\omega)$ between the wave number k and the sinusoidal frequency ω is obtained by solving this Helmholtz equation with appropriate boundary conditions for TM or TE modes. In a waveguide with walls of infinite conductivity the boundary conditions are imposed at the inner radius of the cylindrical wall and result in a well-posed eigenvalue problem whose solution gives the dispersion relation. If the skin depth is small in comparison with the wall thickness and waveguide radius, finite conductivity effects can be incorporated into the analysis by perturbation theory or a variational calculation. The incorporation of finite wall conductivity yields a complex wave number $k(\omega)$

$$k(\omega) = j[k^0(\omega) + \beta(\omega)] + \alpha(\omega) \tag{2.3}$$

where $k^0(\omega)$ is the wave number for perfectly conducting walls and $\beta(\omega)$ is the change in the propagation constant due to finite conductivity. In a good conductor, the $\beta(\omega)$ correction is usually small and can be neglected. However, the $\beta(\omega)$ term may be significant near the cut-off frequency ω_{cut}, where $k^0(\omega_{cut}) = 0$. The $\alpha(\omega)$ term is the attenuation coefficient due to conduction currents within the wall which result in Joule heating. The dispersion relations for a single, hollow, cylindrical conductor of inner radius b and infinite conductivity are given by[15]

$$k_{TM}^0(\omega) = \sqrt{\left(\frac{\omega}{c}\right)^2 - \left(\frac{P_{nm}}{b}\right)^2}$$

$$k_{TE}^0(\omega) = \sqrt{\left(\frac{\omega}{c}\right)^2 - \left(\frac{Q_{nm}}{b}\right)^2} \tag{2.4}$$

where P_{nm} and Q_{nm} denote the m-th root of the Bessel functions $J_n(P_{nm}) = 0$ and $J_n'(Q_{nm}) = 0$ respectively. The integer n denotes the order of the Bessel function. Values of these roots are given in Table I.

TABLE I –Bessel Function Zeros

MODE	P_{nm}	MODE	Q_{nm}
TM_{01}	2.405	TE_{11}	1.841
TM_{11}	3.832	TE_{21}	3.054
TM_{21}	5.136	TE_{01}	3.832
TM_{02}	5.520	TE_{12}	5.331

The frequency at which $k^0(\omega)$ is zero is the *cut-off frequency* $\omega_{cut} = 2\pi f_{cut}$. Modes with frequencies below the cut-off frequency will not propagate in the *perfect* waveguide since the wave number $k^0(\omega)$ is purely imaginary and the electromagnetic wave amplitude is exponentially attenuated with axial distance z. This attenuation is not dissipative as is that associated with wall resistance and conductance in systems with propagating waves. Below the cut-off frequency, the waveguide is analogous to a filter composed of reactive elements. The electromagnetic energy is not irreversibly lost via Joule heating in the wall, but is reflected back to the source. The waveguide acts as a pure reactance to a source driven below the cutoff frequency.

Table II provides the cut-off frequencies f_{cut} calculated from Equation (2.4) for a 1.0-cm inner diameter hollow cylindrical waveguide of infinite conductivity.

TABLE II-Cut-off Frequencies f_{cut} (b = 0.5 cm)

Mode	f_{cut} *GHz*	Mode	f_{cut} *GHz*
TM_{01}	22.95	TE_{11}	17.57
TM_{11}	36.57	TE_{21}	29.14
TM_{21}	49.01	TE_{01}	36.57
TM_{02}	52.68	TE_{12}	50.87

The selection of a 1.0 cm diameter waveguide is dictated by experimental limitations on the laser beam size and the number of conducting filaments that can be generated within the laser beam radius. The TE_{11} mode (H wave) has the lowest cut-off frequency and is the fundamental mode of the circular waveguide. In a waveguide with perfectly conducting walls the eigenfunctions (axial modes) are orthogonal. The proof of this assertion relies upon the imposed boundary conditions at the perfectly conducting wall and the two-dimensional form of Green's second identity. However, due to skin-depth effects in actual conductors, in reality the modes are not orthogonal and may couple. The dispersion relations calculated from equation (2.4) for both the TM and TE modes in a cylindrical waveguide with b=0.5 cm are given in Figures 1 and 2. In the ideal waveguide, the excitation of a single mode at some excitation frequency f would result in that particular mode propagating with the corresponding wave number $k^0_{TM,TE}(f)$ determined from the mode dispersion relation. If the excitation frequency is above the cut-off frequencies of available lower modes, these available modes may be excited as well. In general, the net effect of the coupling is an increase in energy loss to the surrounding wall.

As an example, if one were to excite the TE_{01} mode, which has a cut-off frequency of 36.57 GHz, with an appropriate source at $f = 94$ GHz, the TE_{01} mode would propagate within the waveguide and have a $k^0_{TE} = 1815\ m^{-1}$ (Figure 2). The dispersion relation indicates that the TE_{11}, TE_{21} and TE_{12} modes could be excited at the same frequency which lies above all of their cut-off frequencies (Table II). Coupling to these modes via wall conductivity will weakly attenuate and distort the input signal.

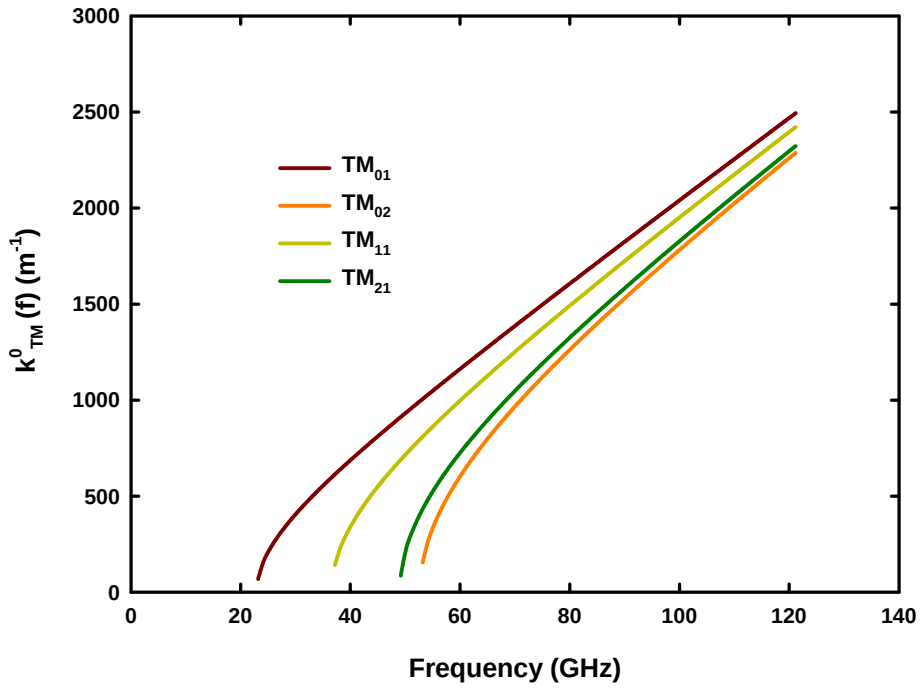

Figure 1 Dispersion relation for TM modes in a cylindrical waveguide of radius 0.5 cm.

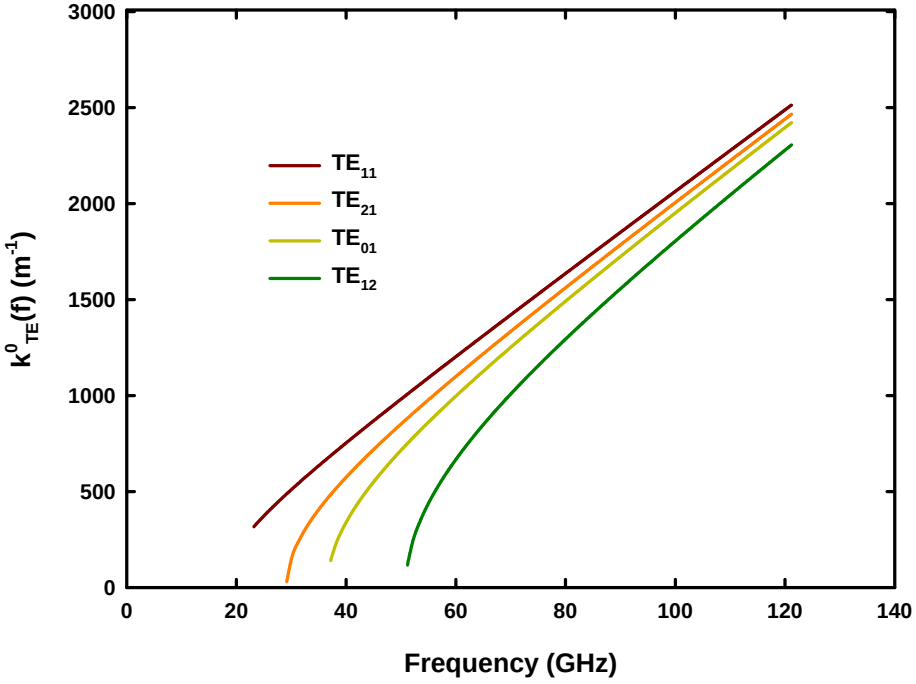

Figure 2 Dispersion relations for TE modes in cylindrical waveguide of radius 0.5 cm.

The reciprocal slope of the dispersion relations provide information about the group and phase velocities of the wave in the waveguide. For propagating modes with $f > f_{cut}$, the phase and group velocities are given by[16]

$$v_{phase}(f) = \frac{2\pi f}{k^0_{TM,TE}} = \frac{c}{\sqrt{1-\left(\frac{f_{cut}}{f}\right)^2}} \qquad v_{group}(f) = \left(\frac{\partial\omega}{\partial k^0}\right)_{TM,TE} = c\sqrt{1-\left(\frac{f_{cut}}{f}\right)^2} \tag{2.5}$$

The electromagnetic wave attenuation for a hollow cylindrical conductor of finite conductivity can be calculated from the power loss to the conductor wall by perturbation theory using the perfectly-conducting eigenfunctions as zero-order solutions. The validity of the calculation depends upon the skin depth being small in comparison to the wall thickness. The attenuation coefficient for the TE and TM modes in a cylindrical waveguide is given by[17]

$$\alpha_{TE}(n,m,f) = \frac{\sqrt{\pi f \mu_0}}{b\eta\sqrt{\sigma}} \frac{1}{\sqrt{1-\left(\frac{f_{cut}}{f}\right)^2}} \left[\left(\frac{f_{cut}}{f}\right)^2 + \frac{n^2}{Q_{nm}^2 - n^2}\right]$$

$$\alpha_{TM}(n,m,f) = \frac{\sqrt{\pi f \mu_0}}{b\eta\sqrt{\sigma}} \frac{1}{\sqrt{1-\left(\frac{f_{cut}}{f}\right)^2}} \qquad \eta \equiv \sqrt{\frac{\mu_0}{\varepsilon_0}} = 376.73\Omega \tag{2.6}$$

These formulae are derived by calculating the time-averaged power flow into the conductor wall. The power loss can be related to an effective surface current and ohmic dissipation of the electromagnetic energy. In the limit of $f >> f_{cut}$, the attenuation coefficients approach the following asymptotic forms for $n = 0$

$$\alpha_{TE}(0,m,f) = \frac{\sqrt{\pi \mu_0}}{a\eta\sqrt{\sigma}} \frac{f_{cut}^2}{f^{3/2}}$$

$$\alpha_{TM}(0,m,f) = \frac{\sqrt{\pi f \mu_0}}{a\eta\sqrt{\sigma}} \tag{2.7}$$

It is to be noted that the attenuation coefficient for all TM modes *increases* with the square root of frequency. However, the attenuation coefficient for all TE_{0m} modes *decreases* as the frequency is increased.

The derivation of these attenuation formulae relies upon the skin depth being small in comparison to the waveguide wall thickness. The spatial variation of the fields normal to the conducting surface is much more rapid than the field variations parallel to the surface. Figure 3 shows calculated skin depths as a function of frequency and conductivity. In this figure we have utilized the conductivity of copper (5.8 x 10^7 S/m) as a reference point and simply reduced the value by a factor of 10^3 or 10^7. The lowest conductivity (5.8 S/m) roughly corresponds to the conductivity of seawater and the skin depth is on the order of millimeters. Thus for materials of this conductivity, the waveguide wall thickness should be several millimeters thick to confine the radiation.

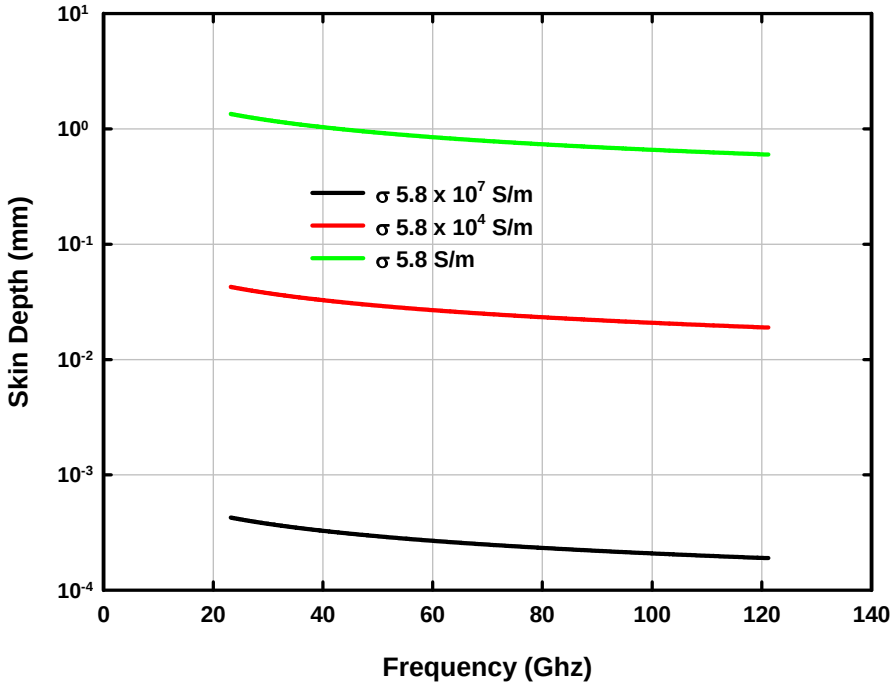

Figure 3 Calculated skin depths vs. frequency.

Calculated attenuation coefficients (decibel/m) are presented in Figures 4 and 5. These calculations were performed for a 0.5 cm radius cylindrical copper waveguide with a wall conductivity of $\sigma_{Cu} = 5.8 \times 10^7 \, S/m$. Note the decrease in the attenuation of the TE_{01} mode (green) with increasing frequency. The attenuation coefficients at a different electrical conductivity σ may be estimated from either of these figures by multiplying the y-axis by the quantity $\sqrt{\frac{\sigma_{Cu}}{\sigma}}$. However, the extrapolation for attenuation coefficients at very low conductivity is suspect. As the wall conductivity is reduced, the skin depth increases and the assumption of a thin transitional layer with rapid decrease in the normal field components becomes invalid. An alternative perturbation method for calculating the loss due to the surrounding wall will be developed below.

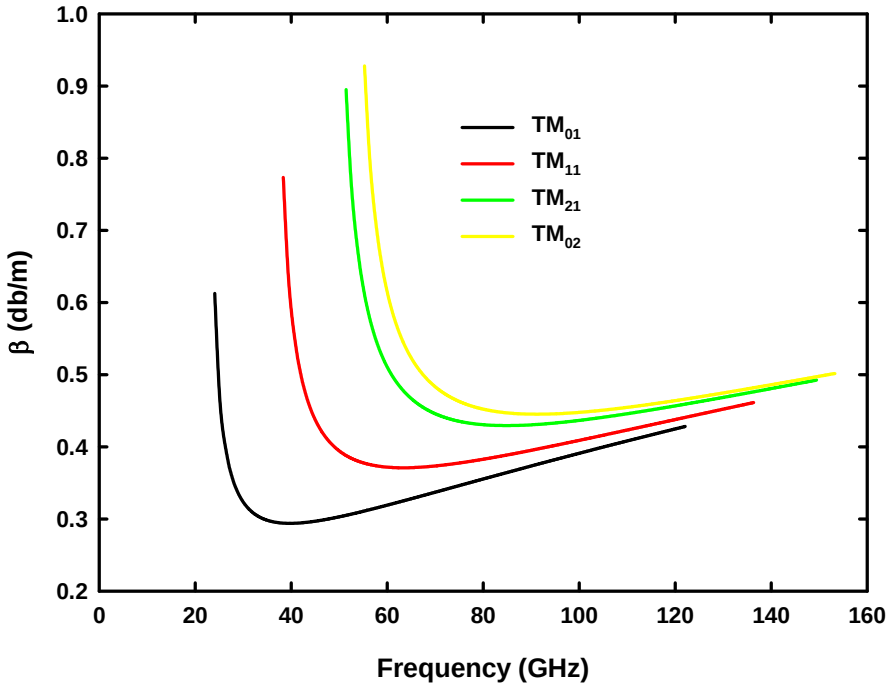

Figure 4 Attenuation coefficients (db/m) for TM modes in cylindrical copper waveguide of radius 0.5 cm. Note the increase in attenuation with frequency.

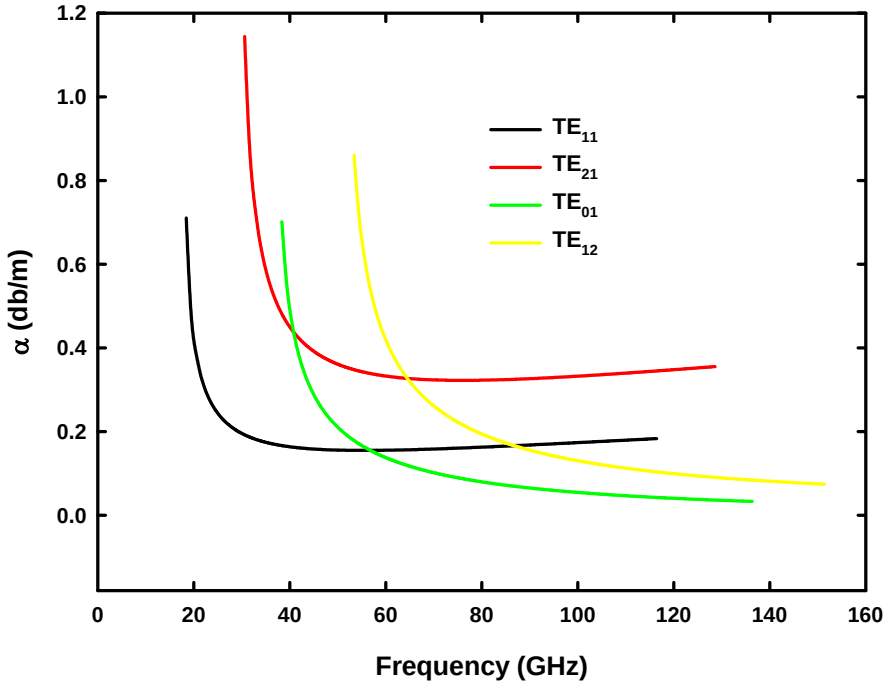

Figure 5 Attenuation coefficients (db/m) for TE modes in a cylindrical copper waveguide of radius 0.5 cm. Note the decrease in attenuation with frequency for the TE_{01} mode.

In order to develop a time-dependent perturbation theory for the attenuation coefficient in a circular cylindrical waveguide, we must first convert Maxwell's equations into time-dependent wave equations. Taking the curl operator ($\nabla\times$) on the Maxwell equations (2.1) results in the following *vector* equations

$$\nabla^2\vec{E} = \mu_0\sigma\frac{\partial\vec{E}}{\partial t} + \frac{1}{c^2}\frac{\partial^2\vec{E}}{\partial t^2} \qquad c \equiv \frac{1}{\sqrt{\mu_0\varepsilon_0}}$$

$$\nabla^2\vec{H} = \mu_0\sigma\frac{\partial\vec{H}}{\partial t} + \frac{1}{c^2}\frac{\partial^2\vec{H}}{\partial t^2} \tag{2.8}$$

If we consider TM or TE waves in a cylindrical waveguide, the respective *axial* field components obey the following *scalar* equations

$$\frac{1}{r}\frac{\partial}{\partial r}\left(r\frac{\partial E_z}{\partial r}\right) + \frac{1}{r^2}\frac{\partial^2 E_z}{\partial\phi^2} + \frac{\partial^2 E_z}{\partial z^2} = \sigma\mu_0\frac{\partial E_z}{\partial t} + \frac{1}{c^2}\frac{\partial^2 E_z}{\partial t^2}$$

$$\frac{1}{r}\frac{\partial}{\partial r}\left(r\frac{\partial H_z}{\partial r}\right) + \frac{1}{r^2}\frac{\partial^2 H_z}{\partial\phi^2} + \frac{\partial^2 H_z}{\partial z^2} = \sigma\mu_0\frac{\partial H_z}{\partial t} + \frac{1}{c^2}\frac{\partial^2 H_z}{\partial t^2} \tag{2.9}$$

These equations are to be solved for $E_z(r,\phi,z,t)$ or $H_z(r,\phi,z,t)$ subject to the following boundary conditions at the waveguide wall $r = b$

$$E_z = 0 \qquad \frac{\partial H_z}{\partial r} = 0 \tag{2.10}$$

These boundary conditions correspond to a perfect conductor at $\mathrm{r} = \mathrm{b}$. If the solutions are assumed to be of the form of equation (2.2) with perfectly conducting walls [$\beta(\omega) = 0, \alpha(\omega) = 0, \sigma = 0$], the axial field components are given by

$$E_z(r,\phi,z,t) = AJ_n\left(\frac{P_{nm}r}{b}\right)\begin{bmatrix}\cos(n\phi)\\ \sin(n\phi)\end{bmatrix}\exp\left(j[\omega t - k_{TM}^0 z]\right)$$

$$H_z(r,\phi,z,t) = AJ_n\left(\frac{Q_{nm}r}{b}\right)\begin{bmatrix}\cos(n\phi)\\ \sin(n\phi)\end{bmatrix}\exp\left(j[\omega t - k_{TE}^0 z]\right) \tag{2.11}$$

These solutions represent stationary waves traveling in the axial direction. The excitation source is at minus infinity. The dispersion relations (2.4) are obtained directly from these **steady-state** solutions.

The transverse field components (E_r, E_ϕ, H_r, H_ϕ) may be obtained from equations (2.11) through Maxwell's equations[18]

$$E_r = -\frac{j}{k_c^2}\left[k_{TM}^0 \frac{\partial E_z}{\partial r} + \frac{\omega\mu_0}{r}\frac{\partial H_z}{\partial \phi}\right] \qquad E_\phi = \frac{j}{k_c^2}\left[\frac{-k_{TM}^0}{r}\frac{\partial E_z}{\partial \phi} + \omega\mu_0 \frac{\partial H_z}{\partial r}\right]$$

$$H_r = \frac{j}{k_c^2}\left[\frac{\omega\varepsilon_0}{r}\frac{\partial E_z}{\partial \phi} - k_{TE}^0 \frac{\partial H_z}{\partial r}\right] \qquad H_\phi = -\frac{j}{k_c^2}\left[\omega\varepsilon_0 \frac{\partial E_z}{\partial r} + \frac{k_{TE}^0}{r}\frac{\partial H_z}{\partial \phi}\right] \tag{2.12}$$

$$k_c^2 \equiv \left(\frac{\omega}{c}\right)^2 - (k_{TE,TM}^0)^2$$

In the notation of reference 18, the propagation constant $\gamma \equiv jk_{TM,TE}^0$.

III. TRANSIENT ANALYSIS OF A CYLINDRICAL PLASMA WAVEGUIDE

For simplicity, we will consider only n=0 modes which implies that the fields are independent of ϕ . Since the differential operator in (2.9) is identical for both axial field variables (E_z, H_z), we may represent the mathematical problem by a single differential equation subject to appropriate boundary and initial conditions

$$\frac{1}{r}\frac{\partial}{\partial r}\left(r\frac{\partial \psi}{\partial r}\right) + \frac{\partial^2 \psi}{\partial z^2} = \sigma\mu_0 \frac{\partial \psi}{\partial t} + \frac{1}{c^2}\frac{\partial^2 \psi}{\partial t^2} \qquad \sigma = \sigma_0 \quad a \le r \le b \quad \sigma = 0 \quad r < a$$

$$\psi(r,0,t) = F(r,t) \quad \psi(r,z,0) = 0 \qquad \left(\frac{\partial \psi}{\partial t}\right)_{t=0} = 0 \qquad \psi = \psi(r,z,t) \quad 0 \le z < \infty \tag{3.1}$$

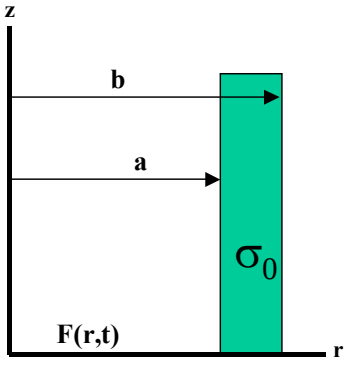

Figure 6 Cylindrical waveguide cross-section.

Figure 6 shows a radial slice of the cylindrical waveguide. The excitation source or incident field at $z = 0$ is represented by the function $F(r,t) = F_1(r)S(\omega t)$. The plasma wall thickness is assumed to be large enough so that the tangential electric field is zero at $r = b$ ($\psi(b,z,t) = 0$). The boundary condition at $r = b$ for the magnetic field intensity (TE modes) is given by equation (2.10). The specified initial conditions correspond to no field within the waveguide region $z \geq 0$ at $t = 0$.

In order to solve equation (3.1) we introduce the asymmetric Fourier Sine transform over z defined by Haberman[19]

$$\hat{f}(r,t,k_z) \equiv \frac{2}{\pi}\int_0^\infty f(r,t,z)\sin[k_z z]\,dz \qquad f(r,t,z) \equiv \int_0^\infty \hat{f}(r,t,k_z)\sin[k_z z]\,dk_z \tag{3.2}$$

Taking the Fourier Sine transform $z \to k_z$ of equation (3.1) yields the following *inhomogeneous* partial differential equation for $\hat{\psi}(r,t,k_z)$

$$\frac{1}{r}\frac{\partial}{\partial r}\left(r\frac{\partial \hat{\psi}}{\partial r}\right) - k_z^2\hat{\psi} + \frac{2}{\pi}k_z F_1(r)S(\omega t) = \sigma(r)\mu_0\frac{\partial \hat{\psi}}{\partial t} + \frac{1}{c^2}\frac{\partial^2 \hat{\psi}}{\partial t^2} \tag{3.3}$$

The time-dependent excitation source of frequency $\omega = 2\pi f$ at $z = 0$ now appears explicitly in the equation. The boundary condition imposed upon the electric field ($\psi(b,t,z) = 0$) suggests that we seek the solution of equation (3.3) for TM modes in the form of an eigenfunction expansion using zero-order Bessel functions of the first kind $J_0(x)$ and time-dependent coefficients $A_n(t,k_z)$

$$\hat{\psi}(r,t,k_z) = \sum_{n=1}^{\infty} A_n(t,k_z)J_0\left(\tfrac{P_{0n}r}{b}\right) \qquad F(r,t) = S(\omega t)\sum_{m=1}^{\infty}\Gamma_m J_0\left(\tfrac{P_{0m}r}{b}\right) \qquad J_0(P_{0n}) = 0 \tag{3.4}$$

where P_{0n} denotes the nth zero (Table I) of $J_0(x)$. The selected eigenfunctions are finite at $r = 0$ and satisfy the imposed boundary condition on the electric field E_z at $r = b$. The eigenfunctions for TE modes (See Eqn. 2.11) would be of the same form, except that the parameter P_{0n} would be replaced by Q_{0n} from Table I. The excitation source $F(r,t)$ is also expanded in equation (3.4) as a Fourier-Bessel series with an assumed time dependence of $S(\omega t)$. The Fourier amplitudes Γ_m of the excitation source are calculated from the following integral

$$\Gamma_m = \frac{1}{N_m}\int_0^b F_1(r')rJ_0\left(\frac{P_{0m}r'}{b}\right)dr' \qquad N_m = \frac{1}{2}b^2J_1^2(P_{0m}) \tag{3.5}$$

where N_m is a normalization factor. In general the Fourier amplitudes may be functions of time. We shall assume that the time-dependence is factorable from the spatial dependence in the excitation source. Figure 7 illustrates the Fourier-Bessel expansion of a possible model incident electric field defined by

$$F_1(r) = E_z^0 H(a-r) \qquad 0 \le r \le a \quad z = 0 \tag{3.6}$$

where $H(a-r)$ denotes the Heaviside step function. This excitation source corresponds to a uniform field over a small circular aperture of radius $r = a$. The model could be used to represent the axial electric field in a cylindrical resonator operating in a TM_{01} mode and with two small holes of radius a on the end caps As the number of terms increases, the Fourier-Bessel series converges in the mean to the incident field. Each Fourier component in the expansion corresponds to a particular eigenmode of the waveguide.

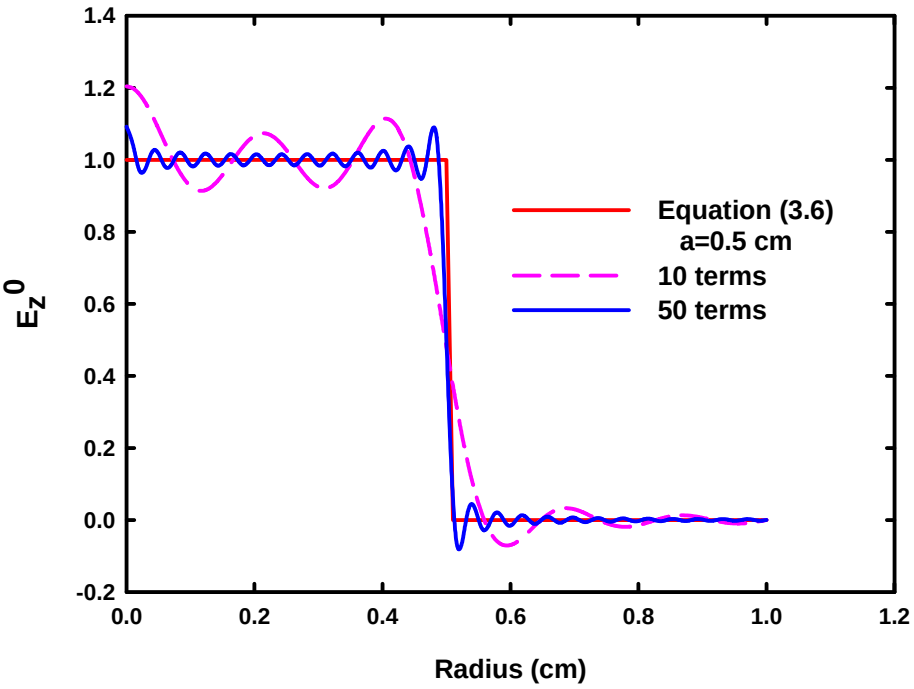

Figure 7 Fourier-Bessel series representation of a uniform incident field at z= 0. The model could represent the axial electric field in a TM_{01} circular resonator with a hole of radius a.

Substitution of equation (3.4) into equation (3.3) yields

$$\sum_{n=1}^{\infty}\left[-\left(\left(\frac{P_{0n}}{b}\right)^2 + k_z^2\right)A_n(t,k_z) + \frac{2k_z}{\pi}S(\omega t)\Gamma_n - \frac{1}{c^2}A_n''(t,k_z)\right]J_0\left(\frac{P_{0n}r}{b}\right) = \sum_{n=1}^{\infty}\sigma(r)\mu_0 A_n'(t,k_z)J_0\left(\frac{P_{0n}r}{b}\right) \tag{3.7}$$

The prime notation denotes time differentiation. Note that the conductivity $\sigma(r)$ is an explicit piecewise continuous function of the radial position r within the waveguide. If the conductivity were zero, the eigen functions $J_0\left(\frac{P_{0n}r}{b}\right)$ would be orthogonal over the interval $[0,b]$ by Sturm-Liouville theory.

If we set the conductivity to zero, the right-hand-side of equation (3.7) becomes zero and the transient model would reduce to an infinite set of linearly independent driven harmonic oscillator equations (3.8) each corresponding to a particular waveguide mode and subject to the initial conditions that $A_n(0,k_z)=0$ and $A_n'(0,k_z)=0$

$$A_n''(t,k_z)+\Omega_n^2\left(k_z\right)A_n(t,k_z)=\frac{2k_zc^2}{\pi}\Gamma_nS(\omega t)\qquad \Omega_n^2\left(k_z\right)\equiv\left(\left(\frac{P_{0n}}{b}\right)^2+k_z^2\right)c^2>0 \tag{3.8}$$

For an arbitrary forcing function $S\left(\omega t\right)$, equation (3.8) is readily solved by taking the Laplace transform over time. The Laplace transform $t\rightarrow s$ is defined by

$$A(s,k_z)\equiv\int_0^\infty A(t,k_z)\exp\left[-st\right]dt=L\left[A\left(t,k_z\right)\right] \tag{3.9}$$

Taking the Laplace transform $t\rightarrow s$ of equation (3.8) and solving for $A_n(s,k_z)$ yields the solution in the $\left[s,k_z\right]$ space

$$A_n(s,k_z)=\frac{2k_z\Gamma_n}{\pi}\frac{c^2}{s^2+\Omega_n^2\left(k_z\right)}\frac{S(s/\omega)}{\omega} \tag{3.10}$$

The inverse Fourier Sine transform $k_z\rightarrow z$ of equation (3.10) recovers the z-dependence.

$$\begin{aligned}A_n\left(s,z\right)&=\frac{2}{\pi}\int_0^\infty\frac{k_z\sin\left[k_zz\right]\Gamma_n}{\left(\left(\frac{s}{c}\right)^2+\left(\frac{P_{0n}}{b}\right)^2\right)+k_z^2}dk_z\left(\frac{S\left(s/\omega\right)}{\omega}\right)\\&=\Gamma_n exp\left[-\frac{z}{c}\sqrt{s^2+\left(\frac{P_{0n}c}{b}\right)^2}\right]\left(\frac{S\left(s/\omega\right)}{\omega}\right)\end{aligned} \tag{3.11}$$

Equation (3.11) is written as the product of two Laplace transforms. One factor $S\left(s/\omega\right)\frac{1}{\omega}$ is the Laplace transform of the excitation source. The exponential factor can be associated with the resolvent or Green's function for Eqn. (3.8). The Laplace inversion (L^{-1}) of the exponential function in (3.11) back to the time domain is accomplished by the following substitution[20]

$$-L^{-1}\left[\exp\left(\frac{-z}{c}s\right)-\exp\left(\frac{-z}{c}\sqrt{s^2+\left(\frac{P_{0n}c}{b}\right)^2}\right)-\exp\left(\frac{-z}{c}s\right)\right]$$

$$=\left[\delta\left(t-\frac{z}{c}\right)-\frac{P_{0n}z}{b\sqrt{t^2-\left(\frac{z}{c}\right)^2}}J_1\left(\frac{P_{0n}c}{b}\sqrt{t^2-\left(\frac{z}{c}\right)^2}\right)H\left(t-\frac{z}{c}\right)\right] \tag{3.12}$$

This Laplace inversion provides a time-dependent Green's function $G(t,z)$ for the n-th mode. The mode evolution for an arbitrary driving function can be obtained by the Laplace transform convolution theorem

$$A_n(t,z)=\int_0^t \Gamma_n G(\tau,z)S\left(\omega[t-\tau]\right)d\tau \tag{3.13}$$

Equation (3.13) may be readily implemented in MathCAD or Mathematica to explicitly calculate the mode evolution for an arbitrary temporal excitation function $S(\omega t)$.

If we assume $S(t)=Sin(\omega t)$, equation (3.10) for $A_n(s,k_z)$ takes the following form

$$A_n(s,k_z)=\frac{2k_z\Gamma_n}{\pi}\frac{c^2}{s^2+\Omega_n^2(k_z)}\left(\frac{\omega}{s^2+\omega^2}\right) \qquad \Omega_n^2(k_z)\equiv c^2\left(\left(\frac{P_{0n}}{b}\right)^2+k_z^2\right) \tag{3.14}$$

This expression can be inverted back to the time domain $s\rightarrow t$ by the inverse Laplace transform to give two terms for $A_n(t,k_z)$

$$A_n(t,k_z)=\frac{2c^2\Gamma_n}{\pi}k_z\left(\frac{\omega Sin(\Omega(k_z)t)-\Omega(k_z)Sin(\omega t)}{\Omega(k_z)\left[\omega^2-\Omega^2(k_z)\right]}\right) \tag{3.15}$$

In order to recover the z-dependence, the inverse Fourier Sine transform must be applied to equation (3.15). The equation is first rearranged as follows

$$A_n(t,k_z)=\frac{2c^2\Gamma_n}{\pi}\left[\frac{\omega k_z\sin\left[\Omega(k_z)t\right]}{\Omega(k_z)\left[\omega^2-\Omega(k_z)^2\right]}-\frac{k_z\sin[\omega t]}{\left(\omega^2-\Omega(k_z)^2\right)}\right] \tag{3.16}$$

The inversion $k_z \rightarrow z$ of the last term depends upon the sign of $\left(\frac{\omega}{c}\right)^2 - \left(\frac{P_{0n}}{b}\right)^2$ and yields two types of solutions:

$$A_n(t,z) = \Gamma_n \exp\left[-z\sqrt{\left(\frac{P_{0n}}{b}\right)^2 - \left(\frac{\omega}{c}\right)^2}\right]\sin(\omega t) \qquad \left(\frac{P_{0n}}{b}\right)^2 - \left(\frac{\omega}{c}\right)^2 > 0$$

$$A_n(t,z) = \Gamma_n \exp\left[-jz\sqrt{\left(\frac{\omega}{c}\right)^2 - \left(\frac{P_{0n}}{b}\right)^2}\right]\sin(\omega t) \tag{3.17}$$

$$= \frac{\Gamma_n}{2}\left[\sin\left(\omega t - k_{TM}^0 z\right) + \sin\left(\omega t + k_{TM}^0 z\right)\right] \qquad k_{TM}^{0\,2} \equiv \left(\frac{\omega}{c}\right)^2 - \left(\frac{P_{0n}}{b}\right)^2 > 0$$

The first equation of (3.17) describes an *evanescent* wave that decays exponentially in the z-direction from the source. This occurs when the excitation frequency ω is below the mode cutoff frequency. The second equation of (3.17) describes traveling waves excited by a source whose frequency is above the mode cutoff frequency. The mode dispersion relation is the same as that given by equation (2.4). The inversion of the first term in equation (3.16) is under investigation.

We will now incorporate the effect of finite conductivity upon the mode propagation and loss. The excitation source is assumed to be of the form $Sin(\omega t)$. Multiplying both sides of equation (3.7) by $J_0\left(\frac{P_{0m} r}{b}\right)$ and noting that the eigenfunctions on the left-hand-side are orthonormal over the interval $[0,b]$ yields

$$\frac{1}{c^2}A_m''(t,k_z) + \frac{\Omega_m^2(k_z)}{c^2}A_m(t,k_z) = \frac{2k_z\Gamma_m}{\pi}Sin(\omega t) - \sum_{n=1}^{\infty}\langle m|\sigma(r,t)|n\rangle A_n'(t,k_z)\frac{\mu_0}{N_m} \tag{3.18}$$

$$\langle m|\sigma(r,t)|n\rangle \equiv \int_0^b J_0\left(\frac{P_{0m} r}{b}\right) r\sigma(r,t) J_0\left(\frac{P_{0n} r}{b}\right) dr$$

Equation (3.18) shows that the first effect of the finite conductivity is to couple the m-th mode with all other waveguide modes. If the conductivity were a constant defined over the interval $[0,b]$, the infinite n-sum on the right-hand-side of (3.18) would reduce to a single diagonal term in which $n = m$ and we would obtain an independent damped harmonic oscillator equation analogous to equation (3.8) for each mode.

An approximate solution for the damping of the m-th mode can be obtained by iteration of equation (3.18). This equation can be rearranged as follows

$$A_m''(t,k_z)+2\gamma_m A_m'(t,k_z)+\Omega_m^2(k_z)A_m(t,k_z)=\frac{2k_z\Gamma_m c^2\sin(\omega t)}{\pi}-c^2\mu_0\sum_{m\neq n=1}^{\infty}\frac{\langle m|\sigma(r,t)|n\rangle}{N_m}A_n'(t,k_z)$$
$$2\gamma_m\equiv\frac{\mu_0 c^2}{N_m}\langle m|\sigma(r,t)|m\rangle \tag{3.19}$$

The approximate solution for the m-th damped mode is constructed by neglecting the mode coupling terms in the sum on the right-hand-side and solving the driven damped oscillator equation by taking the Laplace transform over time.

$$\begin{aligned}A_m(s,k_z)&=\frac{2k_z\Gamma_m c^2}{\pi}\frac{1}{s^2+2\gamma_m s+\Omega_m^2(k_z)}\left(\frac{\omega}{s^2+\omega^2}\right)\\&=\frac{2k_z\Gamma_m c^2}{\pi}\frac{1}{(s+\gamma_m)^2+\Omega_m^2(k_z)-\gamma_m^2}\left(\frac{\omega}{s^2+\omega^2}\right)\end{aligned} \tag{3.20}$$

The z-dependence of $A_m(s,z)$ is recovered by taking the inverse Fourier Sine transform $k_z\to z$ of equation (3.20)

$$A_m(s,z)=\Gamma_m\left(\frac{\omega}{s^2+\omega^2}\right)exp\left[\frac{-z}{c}\sqrt{(s+\gamma_m)^2+\omega_m^2}\right]\qquad\omega_m^2\equiv\left(\frac{P_{0m}c}{b}\right)^2-\gamma_m^2>0 \tag{3.21}$$

The inversion of equation (3.21) back to the time domain is accomplished by the following substitution

$$L^{-1}\left(exp[\frac{-z}{c}\sqrt{(s+\gamma_m)^2+\omega_m^2}]\right)=$$
$$L^{-1}\left(exp\left[\frac{-z}{c}(s+\gamma_m)\right]+exp[\frac{-z}{c}\sqrt{(s+\gamma_m)^2+\omega_m^2}]-exp\left[\frac{-z}{c}(s+\gamma_m)\right]\right) \tag{3.22}$$

The inverse Laplace transform of equation (3.22) may be written as a product of two time-dependent functions using the Laplace transform substitution theorem[21]

$$L^{-1}\left[f(s+\gamma)\right]=exp(-\gamma t)f(t) \tag{3.23}$$

Using relation (3.23) and Churchill's Tables of Laplace transforms[20], the time-domain solution is given by

$$exp\left[-\gamma_m t\right]\left[\delta\left(t-\frac{z}{c}\right)-H\left(t-\frac{z}{c}\right)\frac{\omega_m z}{c\sqrt{t^2-\left(\frac{z}{c}\right)^2}}J_1\left(\omega_m\sqrt{t^2-\left(\frac{z}{c}\right)^2}\right)\right] \tag{3.24}$$

Equation (3.24) provides the Green's function or response function associated with the m-th mode. The temporal evolution of the mode coefficient $A_m(t,z)$ can be calculated from the Laplace convolution integral for the sinusoidal input $S(t)=Sin(\omega t)$

$$\Gamma_m\int_0^t exp\left[-\gamma_m\tau\right]\left[\delta\left(\tau-\frac{z}{c}\right)-H\left(\tau-\frac{z}{c}\right)\frac{\omega_m z}{cF(\tau,z)}J_1\left(\omega_m F(\tau,z)\right)\right]S\left[\omega(t-\tau)\right]d\tau \tag{3.25}$$

$$F(\tau,z)\equiv\sqrt{\tau^2-\left(\frac{z}{c}\right)^2}$$

Since the excitation source $S(\omega t)$ is a time-dependent sine function, the Dirac delta function in equation (3.25) reduces the integration over the first term to a damped harmonic oscillator solution

$$\Gamma_m exp\left[-\gamma_m\frac{z}{c}\right]Sin\left[\omega\left(t-\frac{z}{c}\right)\right] \qquad t\geq\frac{z}{c} \tag{3.26}$$

This term represents a spatially damped wave of initial amplitude Γ_m traveling at the speed of light within the plasma tube in the positive z-direction. This term corresponds to a standard perturbation treatment in which the attenuation due to wall conductivity for a travelling sine wave as an initial condition is calculated. In the coupled metal-plasma tube model, the amplitude would be determined from the steady-state mode at the aperture $z=0$. The second term in (3.25) has both a decay and oscillatory behavior associated with the Bessel function J_1. The sinusoidal driving term $Sin\left[\omega(t-\tau)\right]$ can be written as two terms

$$Sin\left[\omega(t-\tau)\right]=Sin\left[\omega t\right]Cos\left[\omega\tau\right]-Cos\left[\omega t\right]Sin\left[\omega\tau\right] \tag{3.27}$$

Substitution of Eqn. (3.27) into Eqn. (3.25) gives the following solution

$$A_m(t,z) = \Gamma_m \exp\left(-\gamma_m \frac{z}{c}\right)\left[Sin\left[\omega\left(t-\frac{z}{c}\right)\right] - Sin[\omega t] I_{\cos}(t,z) + Cos[\omega t] I_{\sin}(t,z)\right]$$

$$I_{\cos}(t,z) \equiv \int_0^t Cos[\omega\tau] \frac{H\left(\tau-\frac{z}{c}\right)\omega_m z}{c\sqrt{\tau^2-\left(\frac{z}{c}\right)^2}} J_1\left(\omega_m\sqrt{\tau^2-\left(\frac{z}{c}\right)^2}\right) d\tau \tag{3.28}$$

$$I_{\sin}(t,z) \equiv \int_0^t Sin[\omega\tau] \frac{H\left(\tau-\frac{z}{c}\right)\omega_m z}{c\sqrt{\tau^2-\left(\frac{z}{c}\right)^2}} J_1\left(\omega_m\sqrt{\tau^2-\left(\frac{z}{c}\right)^2}\right) d\tau$$

This solution is difficult to interpret. However, we can consider some limiting cases. For z=0 and all time t > 0, equation (3.28) reduces to $\Gamma_m Sin(\omega t)$ which corresponds to the specified boundary condition at z=0. In the limit of $t \to \infty$, the integrals go to zero and the solution becomes a spatially damped traveling wave of the form $\Gamma_m \exp\left(\frac{-\gamma_m z}{c}\right) Sin\left(\omega t - \frac{z}{c}\right)$. For intermediate values of z and t, the signal propagates at the speed of light c. The Heaviside function $H\left(\tau-\frac{z}{c}\right)$ introduces temporal retardation into the signal propagation. The amplitude seen by a field detector or probe at some intermediate position and time is composed of sinusoidal oscillations at frequency ω modulated by the Bessel function integrals. For specified values of z and t, these integrals can be evaluated numerically. Figure 8 shows the time dependence of the Green's function (integrand) for the $I_{\cos}(z,t)$ component. Figure 9 depicts the integral of this component and its contribution to the signal amplitude at the same position. The transient contribution to the signal is on the order of 10-15 %.

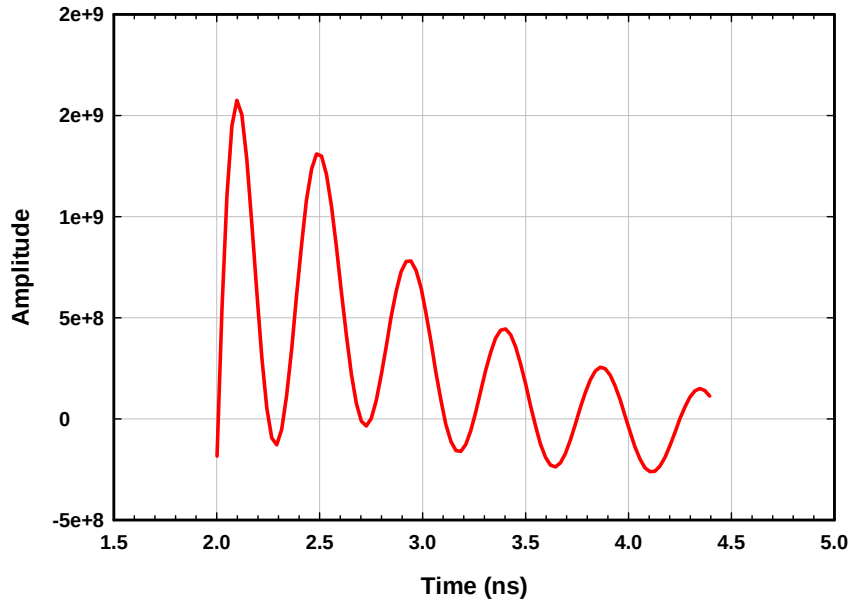

Figure 8 Green Function $I_{\cos}\left(z,t\right)$ component at z=50 cm. and f=1.0 GHz

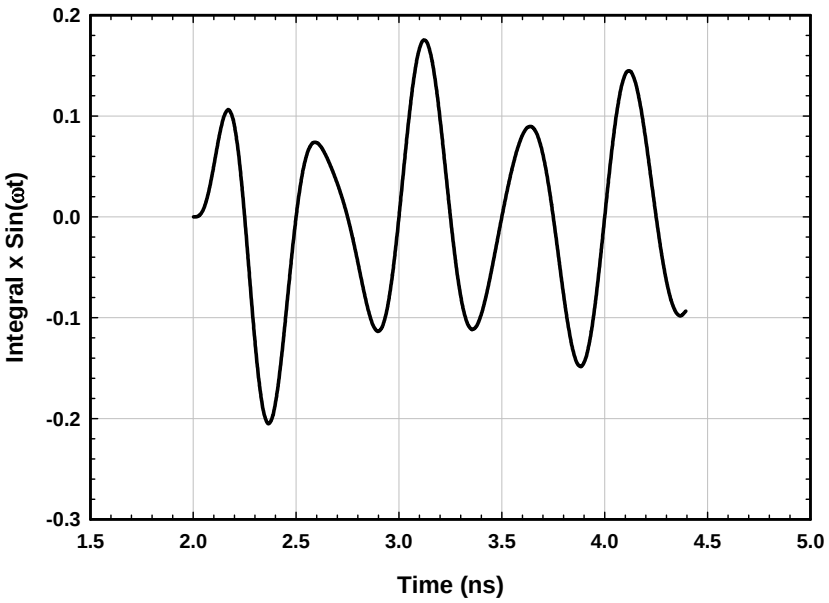

Figure 9 Integral contribution to signal amplitude at z=50 cm. and f=1.0 GHz.

IV. FINITE-ELEMENT COMPUTATIONS

In order to validate the analytic model described here, some preliminary numerical simulations were performed using the finite-element code Comsol 3.5. The geometry of the model is depicted in Figure 10. The model geometry assumes a perfectly-conducting metal tube (PEC) of radius 5 mm is connected to a plasma tube of the same interior radius with a wall thickness .5 mm. Specified TM and TE modes above the tube cut-off frequencies can be launched from the excitation port and propagated into the plasma region. The attenuation is determined by numerically integrating the axial Poynting vector, which describes the power flow, over the waveguide cross section at the plasma inlet port and at a second station located 5 cm from the end of the 10 cm plasma tube. An attenuation coefficient α (1/m) is derived from the integrated power ratio and the assumption of an exponential decay over the propagation distance of 5.0 cm. The preliminary calculations were done assuming steady-state propagation in order to determine the finite-element size, grid and memory requirements for numerical convergence.

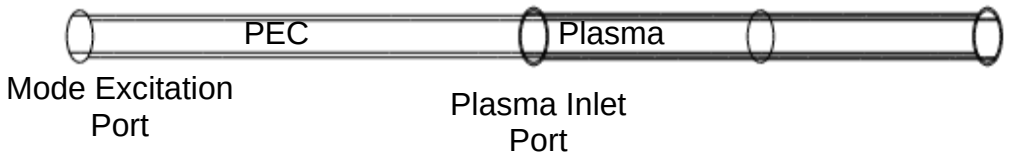

Figure 10 Geometry of numerical model.

In order to confine the wave within the 50 S/m plasma region, the excitation frequencies were selected by requiring the skin depths be less than 0.5 mm. This plasma wall thickness would correspond roughly to three closely packed circular arrays of 100-150 μm laser induced filaments. The results of these calculations are given in Table III and Figure 11.

Table III Attenuation Calculations TM_{01} Mode

Excitation Frequency (GHz)	Skin Depth (mm) σ = 50 S/m	Numerical α (1/m)	Standard Perturbation α (1/m)	α (1/m) Equation (3.19)
25	.45	45.6	59.5	53.9
30	.41	42.1	40.1	53.6
35	.38	44.2	37.0	53.2
40	.36	47.6	36.4	52.6
45	.34	51.2	36.8	51.3
50	.32	55.0	37.6	50.6
55	.30	58.5	38.5	49.9
60	.29	62.4	39.6	49.2

The standard perturbation theory underestimates the attenuation in the plasma waveguide. This is not unexpected, since the underlying assumption for applying the perturbation model is that the skin depth is small in comparison with the plasma wall thickness. The numerical power integration shows an increase in attenuation with frequency. The loss is on the order of 360 to 550 db/m. Experiments conducted with this geometry and frequency range would not be able to detect a propagating signal.

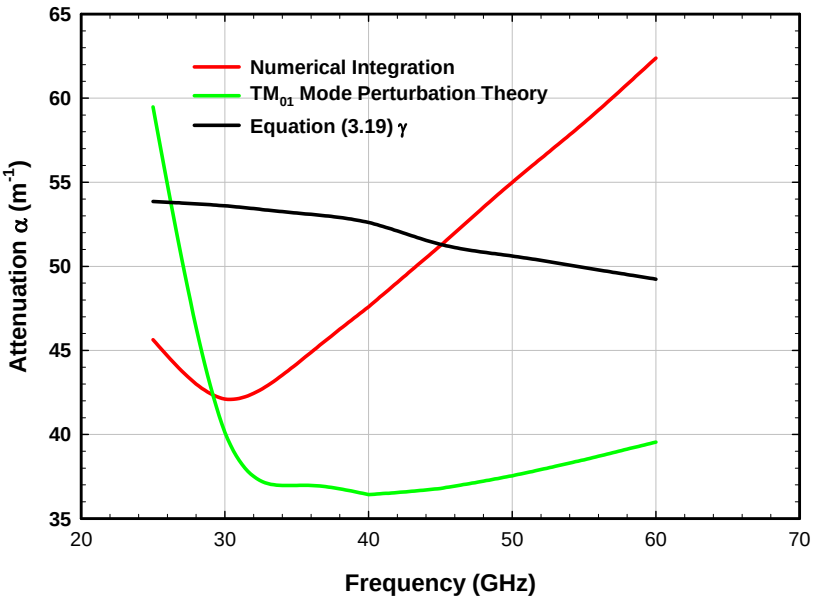

Figure 11 TM_{01} mode attenuation for waveguide of radius 5 mm.

Perturbation theory indicates that the loss is inversely proportional to the waveguide radius. Figure 12 shows the calculated attenuation for a TE_{11} mode in a 6.0 cm diameter plasma waveguide with a 2 mm thick wall. Under these conditions the perturbation theory and the numerical power integration are in reasonable agreement and the attenuation is reduced by an order of magnitude.

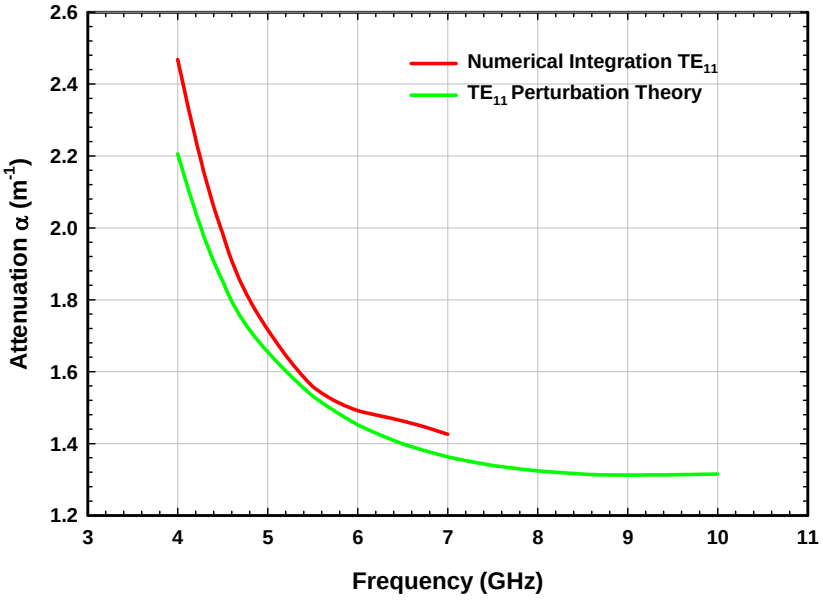

Figure 12 Calculated steady-state attenuation in a plasma (50 S/m) waveguide of radius 3 cm.

V. CONCLUSION

An analytic model to describe the transient propagation of an electromagnetic wave inside a hollow constant conductivity plasma annular tube has been formulated utilizing integral transform techniques. The model provides insight into the wave attenuation, the nature of the evanescent and propagating modes (Eqn. 3.17), the dispersion relations and waveguide excitation. The key result of the time-dependent analysis is equation (3.24) which provides a Green's function for the solution of the interior propagation problem. The Green's function reveals that the transient signals seen by a field detector have oscillatory components of the same frequency as the excitation source, but with time-dependent modulated amplitudes (e.g. Fig. 9) that depend upon the distance from the excitation source. The Green's function is a complex entity and how it relates to what we measure in any particular experiment is under investigation. Although the Green's function developed here is only applicable to the specified geometry of the cylindrical waveguide model, the integral techniques utilized in the development can be extended to other geometries. We propose to use similar techniques for the open waveguide to understand launching and possible surface wave formation on the laser-generated plasma filaments.

Some preliminary numerical calculations on closed plasma waveguides have been performed utilizing a finite-element code. The simplest and probably the best possible configuration for guided wave propagation is a steady-state. Published papers[2-3] have utilized conventional perturbation theory, which assumes a given mode is propagating within the waveguide, to predict the attenuation of that mode within the hollow plasma tube. We have compared both the perturbation theory and the finite-element calculations for wave attenuation in a 50 S/m plasma. In order to confine the wave within the waveguide over the 4-10 GHz frequency, the annular plasma thickness should be on the order of a few millimeters with a waveguide radius of 3.0 cm. The calculated attenuation in this configuration is on the order of 12-20 db/m for the TE_{11} mode. For this particular geometry and mode, the perturbation calculations and the numerical integrations agree reasonably well as shown in Figure 12. As the waveguide diameter is reduced, the attenuation increases. At the higher frequencies and for smaller diameter waveguide, the perturbation theory and the numerical computations for the attenuation are in poor agreement as shown in Figure 11.

Finally, we note that an alternative approach to guiding the electromagnetic wave is to use a waveguide whose radius is much larger than the wavelength of interest. The guiding mechanism is based on the effect of total reflection at the plasma-air interface. Signals at 38 GHz have been directed over distance of 60 m by this approach which is referred to as a sliding mode[2-3].

Part of the motivation for doing the steady-state calculations and comparing them with perturbation theory is to confirm the accuracy and predictive character of the numerical model. The annular tube waveguide problem has both closed-form and perturbation solutions which can be compared with the numerical results to determine the appropriate input conditions such as grid size, plasma wall thickness, propagation length and outer region boundary conditions. If the annular plasma wall were replaced with a ring of plasma filaments, there are no analytic expressions for the solutions to compare the numerical predictions with. The problem is also complicated by the fact that the computational domain is now open to free space and the wave can "leak" out into the surroundings. Thus, one of our first objectives was to establish the conditions under which the numerical work agrees with a known analytic model and where it becomes invalid.

REFERENCES

1. M. Chateauneuf, S. Payeur, J. Dubois, and J.-C. Kieffer, "Microwave guiding in air by a cylindrical filament array waveguide," *Applied Physics Letters* 92, 091104 (2008).
2. A. E. Dormidonov, V.V. Valuev, V.L. Dmitriev, S.A. Shlenov, V.P. Kandidov, "Laser Filament Induced Microwave Waveguide in Air," *Proc. of SPIE* Vol. 6733, 67332S-1 (2007) doi: 1117/12.753246.
3. V.V. Valuev, A.E. Dormidonov, V. P. Kandidov, S.A. Shlenov, V.N. Kornienko,and V.A. Cherepenin, "Plasma Channels Formed by a Set of Filaments As a Guiding system for Microwave Radiation," *Journal of Communications Technology and Electronics*, Vol. 55, No. 2, pp 208-214 (2010).
4. Roman R. Musin, Mikhail N. Shneider, Aleksei M. Zheltikov, and Richard B. Miles, "Guiding radar signals by arrays of laser-induced filaments: finite-difference analysis," *Applied Optics*, vol. 46, No. 23, pp 5593-5597 (2007).
5. G.V. Naidis, "On propagation characteristics of electromagnetic waves along a plasma filament," *Journal of Physics D: Applied Physics*, Vol. 34, L103-L104 (2001).
6. G. Goubau, "Surface Waves and Their Application to Transmission Lines," *Journal of Applied Physics*, Vol. 21, pp 1119-1128 (1950).
7. H. D. Ladouceur, A.P. Baronavski, D. Lohrmann, and P.W. Grounds, "Electrical conductivity of a femtosecond laser generated plasma channel in air," *Optics Communications*, 189, pp 107-111 (2001).
8. V.D. Zvorykin, A.O. Levchenko, N.N. Ustinovskii, and I.V. Smetanin, "Transfer of Microwave Radiation in Sliding Mode Plasma Waveguides," JETP Letters, Vol. 91, No. 5, pp 226-230 (2010).
9. Igor V. Smetanin, Vladimir D. Zvorykin, Alexey O. Levchenko, and Nikolay N. Ustinovsky, "Transfer of Microwave Radiation in Sliding Modes of Plasma Waveguides," *Journal of Russian Laser Research*, Vol. 31, No. 5, pp 495-508 (2010).
10. N.A. Bogatov, A.I. Kuznetsov, A.I. Smirnov, and A.N. Stepanov, "Channeling of microwave radiation in a double line containing a plasma filament produced by intense femtosecond laser pulses in air," *Quantum Electronics*, Vol. 39(10), pp 985-988 (2009).
11. Hirotomo Nakajima, Kazuhisa Hashimoto, Michiteru Yamaura, Yoshinori Shimada, Masayuki Fujita, and Kazuo A. Tanaka, "Microwave Propagation via Laser Plasma Channels," *Plasma and Fusion Research: Rapid Communications*, Vol. 2, 012/1-3 (2007).
12. M.N. Shneider, A.M. Zheltkov, and R.B. Miles," Long-Lived laser-induced microwave plasma guides in the atmosphere: Self-consistent plasma-dynamic analysis and numerical simulations," *Journal of Applied Physics*, Vol. 108, 033113/1-7 (2010).
13. M.N. Shneider, A.M. Zheltikov, and R.B. Miles, "Tailoring the air plasma with a double laser pulse," *Physics of Plasmas*, Vol. 18, 063509/1-19 (2011).
14. S. Ramo, J.R. Whinnery, & T. Van Duzer, Fields and Waves in Communication Electronics, 3rd edition, John Wiley & Sons, New York, NY, pp 395-455 (1994).
15. G.F. Miner, Lines and Electromagnetic Fields for Engineers, Oxford University Press, New York, NY, pp 783-798 (1996).
16. Ibid. p 788 & p 796.
17. S. Ramo, J.R. Whinnery, & T. Van Duzer, Fields and Waves in Communication Electronics, 1st edition, John Wiley & Sons, New York, NY, pp 432-434 (1965).
18. Ibid. p 415.
19. R. Habermann, Elementary Applied Partial Differential Equations with Fourier Series and Boundary Value Problems, Prentice-Hall, Englewood Cliffs, NJ, p 368 (1983).

20. R. Churchill, Operational Mathematics, McGraw-Hill, New York, NY, Table A-2, item 92, p 464, (1972).
21. Ibid. p 16